

Universal behaviour of shock precursors in the presence of efficient cosmic-ray acceleration

B. Reville*, A. R. Bell

Clarendon Laboratory, University of Oxford, Parks Road, Oxford OX1 3PU, United Kingdom

Accepted ... Received ...

ABSTRACT

The self-consistent interaction between energetic particles and self-generated hydro-magnetic waves in a cosmic-ray pressure dominated plasma is considered. Using a three-dimensional hybrid MHD-kinetic code, which utilises a spherical harmonic expansion of the Vlasov-Fokker-Planck equation, high resolution simulations of the magnetic field growth including feedback on the cosmic rays are carried out. It is found that for shocks with high cosmic-ray acceleration efficiency, the magnetic fields become highly disorganised, resulting in near isotropic diffusion, independent of the initial orientation of the ambient magnetic field. The possibility of sub-Bohm diffusion is demonstrated for parallel shocks, while the diffusion coefficient approaches the Bohm limit from below for oblique shocks. This universal behaviour suggests that Bohm diffusion in the root mean squared field inferred from observation may provide a realistic estimate for the maximum energy acceleration timescale in young supernova remnants. Although disordered, the magnetic field is not self-similar suggesting non-uniform energy dependent behaviour of the energetic particle transport in the precursor. Possible indirect radiative signatures of cosmic-ray driven magnetic field amplification are discussed.

Key words: acceleration of particles – (ISM:) cosmic rays – plasmas – instabilities.

1 INTRODUCTION

There is a growing wealth of observational evidence that non-linear amplification of magnetic fields occurs at the outer shocks of supernova remnants, both upstream and down (Achterberg et al. 1994; Vink & Laming 2003; Bamba et al. 2005; Rakowski et al. 2011). This discovery represents a significant development in the theories of particle acceleration and the resulting non-thermal emission from supernova remnants. However, despite the fact that almost every attempt to model the non-thermal spectra from young supernova remnants in recent years has incorporated or inferred some level of field amplification, a detailed understanding of the underlying mechanisms that produce such strong fields is still lacking. This can probably be attributed to the complexity of the problem, which, being highly non-linear, requires numerical modelling of processes occurring on a variety of length-scales.

The amplification of magnetic fields to levels far in excess of typical interstellar medium values is advantageous for a number of reasons. First, it seems essential to account for the x-ray synchrotron emission, its short time scale variability, and its localisation to narrow filaments close to the

shock. Second, it is central to explaining the origin of cosmic rays with energies in excess of 10^{15} eV. While the former can in principle be accounted for via fluid instabilities occurring at the shock itself and the region immediately downstream (e.g. Guo et al. 2012), the latter requires strong fields upstream of the shock that can only be produced from instabilities driven by energetic particles streaming ahead of the shock (e.g. Achterberg 1983; Bell 2004). While the non-resonant hybrid (NRH) instabilities described in Bell (2004, 2005) are believed to have the fastest growth rates, whether the resulting short-wavelength structures can significantly influence the highest energy particles has yet to be verified (Bell 2004; Reville et al. 2008).

In this paper, we report on numerical simulations of the interaction between streaming cosmic rays and the thermal plasma upstream of the shock, including a self-consistent treatment of the cosmic rays. The thermal plasma is treated using an MHD fluid approach while the cosmic ray evolution is calculated using a spherical harmonic expansion of the Vlasov-Fokker-Planck equation.

The outline of the paper is as follows. In the next section we introduce the relevant equations and the spherical harmonic expansion that is central to the approach used in this paper. From the resulting equations, the standard expressions for particle drifts and fluxes in the diffusion ap-

* E-mail: b.reville1@physics.ox.ac.uk

proximation are derived. These form the basis for many of the approximations required to self-consistently model the essential processes occurring in the precursor of an efficiently accelerating shock. Section 3 describes the numerical scheme and the simulation results are presented in section 4. We conclude with a summary of the main conclusions and additional discussion.

2 PARTICLE TRANSPORT AND FLUXES

The study of particle acceleration and magnetic field amplification in supernova precursors is essentially one of magnetohydrodynamics. Due to the large length-scales associated with the energetic cosmic rays, their interactions with the background field are mediated by the magnetic fluctuations supported by the background plasma. However, it is the currents provided by the cosmic-rays that often play the dominant role in determining the evolution of the magnetic field in these precursors. We seek an effective numerical method to model the evolution of the cosmic rays in self-generated hydromagnetic waves and structures. For non-relativistic shocks $u_{\text{sh}} \ll c$, it is generally accepted that efficient scattering maintains a quasi-isotropic phase space distribution, at least to order u_{sh}/c . In a previous paper (Reville & Bell 2012), a particle in cell type numerical scheme was adopted to treat the cosmic ray evolution (see also Zachary 1987; Lucek & Bell 2000). Maintaining an isotropic distribution in multi-dimensions turned out to be computationally expensive, with the number of particles per cell required to achieve the desired level of isotropy becoming prohibitively large for simulations in three spatial dimensions.

Recently Bell et al. (2011) performed test particle simulations of cosmic-ray acceleration at oblique shocks in one dimension. The numerical scheme involved a spherical harmonic expansion of the distribution in momentum space based on the KALOS code previously developed for simulations of laser plasma interactions (Bell et al. 2006). In this paper, we describe the full three dimensional expansion, which has been coupled to an MHD code. We adopt the mixed-frame coordinate system commonly used in astrophysics, where momentum variables are measured in the local fluid frame

$$\frac{\partial f}{\partial t} + (\mathbf{u} + \mathbf{v}) \cdot \nabla f - p \mathbf{E} \cdot \frac{\partial f}{\partial \mathbf{p}} - [(\mathbf{p} \cdot \nabla) \mathbf{u}] \cdot \frac{\partial f}{\partial \mathbf{p}} + e v \cdot \left(\mathbf{B} \times \frac{\partial f}{\partial \mathbf{p}} \right) = \mathcal{C}(f) , \quad (1)$$

accurate to second order in u/c (Kirk 1994). In this non-inertial frame an effective electric field term is introduced (cf. Skilling 1975):

$$\mathbf{E} = \frac{1}{c} \left[\frac{\partial \mathbf{u}}{\partial t} + (\mathbf{u} \cdot \nabla) \mathbf{u} \right].$$

We have also kept the third order term $(\mathbf{u} \cdot \nabla) \mathbf{u}$ simply because the resulting expression for the electric field can be inferred from the momentum equation of magnetohydrodynamics, which turns out to be convenient when included in the code. $\mathcal{C}(f)$ represents the usual Fokker-Planck small angle scattering term (e.g. Chandrasekhar 1943). The advantage of using the mixed coordinates system is that the resulting collisions, as given by $\mathcal{C}(f)$, are elastic and isotropic

in the local frame, in the sense that they are proportional to the angular component of the Laplacian in spherical coordinates. Since the spherical harmonics are themselves solutions to Laplace's equation, the resulting collision term takes a very simple form.

Defining $f_\ell^{-m} = (f_\ell^m)^*$ the expansion takes the following form:¹

$$f(p, \theta, \varphi) = \sum_{\ell=0}^{\infty} \sum_{m=-\ell}^{\ell} f_\ell^m(p) P_\ell^{|m|}(\cos \theta) e^{im\varphi} \quad (2)$$

which, on substitution into equation (1), can be used to derive a set of coupled differential equations. These equations are quite lengthy, and for clarity they are written in single column form in the appendix.

To motivate the various approximations that are made later in the simulations, we demonstrate how the well known transport equation is reproduced from the full expansion. For this purpose, it is necessary to retain only terms $\ell < 2$. In the full numerical simulations, many more terms are used.

Defining $f = f_0 + \mathbf{f}_1 \cdot \mathbf{p}/p$ where

$$f_0 = f_0^0, \quad f_x = f_1^0, \quad f_y = -2\Re f_1^1, \quad f_z = 2\Im f_1^1$$

and neglecting the terms associated with \mathbf{E} above (which are second order in u/c), a somewhat tedious calculation shows that:

$$\frac{\partial f_0}{\partial t} + \mathbf{u} \cdot \nabla f_0 + \frac{v}{3} \nabla \cdot \mathbf{f}_1 - \frac{1}{3} (\nabla \cdot \mathbf{u}) p \frac{\partial f_0}{\partial p} = 0 , \quad (3)$$

$$\begin{aligned} \frac{\partial \mathbf{f}_1}{\partial t} + (\mathbf{u} \cdot \nabla) \mathbf{f}_1 + v \nabla f_0 + \mathbf{\Omega} \times \mathbf{f}_1 &= \frac{\nabla u_i}{5p^3} \frac{\partial (p^4 f_i)}{\partial p} \\ &+ \frac{1}{5} \frac{\partial \mathbf{u}}{\partial x_i} p^2 \frac{\partial}{\partial p} \left(\frac{f_i}{p} \right) + \frac{1}{5} (\nabla \cdot \mathbf{u}) p^2 \frac{\partial}{\partial p} \left(\frac{\mathbf{f}_1}{p} \right) - \nu \mathbf{f}_1 , \end{aligned} \quad (4)$$

where $\mathbf{\Omega} = e\mathbf{B}/\gamma mc$ is the directional rotational frequency, ν is the collision frequency and summation over repeated index $i = x, y, z$ is implied. In what follows we assume all particles are ultra-relativistic, and set everywhere $v = c$. Making the usual assumption that the first order terms react on a shorter timescale than the zeroth order component, we take a steady state solution for \mathbf{f}_1 . Retaining only terms to first order in u/c leaves

$$c \nabla f_0 + \mathbf{\Omega} \times \mathbf{f}_1 = -\nu \mathbf{f}_1 ,$$

which can be used to remove the \mathbf{f}_1 dependence in the equation (3) to give

$$\begin{aligned} \frac{\partial f_0}{\partial t} + \mathbf{u} \cdot \nabla f_0 &= \frac{1}{3} (\nabla \cdot \mathbf{u}) p \frac{\partial f_0}{\partial p} \\ &+ \nabla \cdot \left\{ \frac{D_B}{(1+h^2)} [\nabla f_0 + \mathbf{h}(\mathbf{h} \cdot \nabla f_0) - \mathbf{h} \times \nabla f_0] \right\} , \end{aligned} \quad (5)$$

where $\mathbf{h} = \mathbf{\Omega}/\nu$ is the hall parameter, and $D_B = c^2/3\nu$ the usual Bohm diffusion coefficient. It can clearly be seen that in the relevant limits, the transport equation reduces to the well-known forms for parallel shocks

$$\frac{\partial f_0}{\partial t} + \mathbf{u} \cdot \nabla f_0 = \frac{1}{3} (\nabla \cdot \mathbf{u}) p \frac{\partial f_0}{\partial p} + \nabla \cdot (D_B \nabla f_0) \quad (6)$$

¹ For a more rigorous discussion of this expansion see Tzoufras et al. (2011) and references therein.

and perpendicular shocks

$$\frac{\partial f_0}{\partial t} + \mathbf{u} \cdot \nabla f_0 = \frac{1}{3} (\nabla \cdot \mathbf{u}) p \frac{\partial f_0}{\partial p} + \nabla \cdot [D_{\perp} (\nabla - \mathbf{h} \times \nabla) f_0] ,$$

where $D_{\perp} = D_B (1 + h^2)^{-1}$ (Bell 2008).

We seek steady-state solutions, which will later be used to initialise the simulations. In the shock frame, the upstream plasma moves in the positive x direction with uniform speed u_{sh} , and only gradients in this direction are considered. Without loss of generality, a steady magnetic field is taken to lie in the $x - z$ plane (i.e. $\mathbf{h} = h_x \hat{\mathbf{x}} + h_z \hat{\mathbf{z}}$). The resulting upstream steady state solution is

$$f_0(x, p) = f_0(0, p) \exp\left(\int \kappa dx\right), \text{ with } \kappa = \frac{u_{\text{sh}}}{D_B} \frac{1 + h^2}{1 + h_x^2} \quad (7)$$

and the associated fluxes

$$\mathbf{f}_1(x, p) = \frac{3u_{\text{sh}}}{c} \left[-\hat{\mathbf{x}} + \frac{h_z}{1 + h_x^2} \hat{\mathbf{y}} - \frac{h_x h_z}{1 + h_x^2} \hat{\mathbf{z}} \right] f_0(x, p) . \quad (8)$$

In the limit that the amplitude of the scattering waves (or ν) does not increase significantly over a distance $\sim \kappa^{-1}$, the results reduce to equations (5) and (6) of Bell et al. (2011). However, small wavelength modes are in principle excited by the NRH instability of Bell (2004), with maximum growth rate (for quasi-parallel shocks)

$$\gamma_{\text{nr}} = \frac{1}{2} \frac{n_{\text{cr}}}{n_{\text{th}}} \frac{u_{\text{sh}}}{v_A} \Omega$$

such that the number of exponential growth factors in amplitude of magnetic fluctuations over a distance equal to the fluid crossing time of κ^{-1} is

$$\gamma_{\text{nr}} / \kappa u_{\text{sh}} = \frac{n_{\text{cr}}}{n_{\text{th}}} \frac{c}{u_{\text{sh}}} \frac{c}{v_A} \frac{h}{6} \frac{1 + h_x^2}{1 + h^2}$$

For efficient shock acceleration, this number can exceed unity. In fact, at the highest energies, it must exceed unity if magnetic fields are to be amplified upstream.

3 NUMERICAL SCHEME

The numerical scheme is a natural extension of earlier hybrid MHD-kinetic work based on the MHD code used in Reville et al. (2008), with the particle-in-cell approach of Reville & Bell (2012) replaced by a Vlasov-Fokker-Planck routine. The full expansion of equation (A1) is solved numerically using a third order Runge-Kutta method. Making use of the orthogonality relations of the spherical harmonics, it follows that the cosmic-ray particle and current density, measured in the local fluid frame, are

$$n = q \int d^3 p f = 4\pi \int dp p^2 f_0^0 \quad (9)$$

and

$$\mathbf{j}'_{\text{cr}} = q \int d^3 p \mathbf{v} f = \frac{4\pi}{3} q \int dp p^2 v \begin{pmatrix} f_1^0 \\ -2\Re(f_1^1) \\ 2\Im(f_1^1) \end{pmatrix} . \quad (10)$$

The MHD equations, modified by the presence of cosmic rays have been described in detail elsewhere (Zachary 1987; Bell 2004), but we repeat them here for completeness. The standard MHD momentum equation is supplemented with

the additional effect of the return current induced by the cosmic-ray streaming, giving

$$\rho \frac{d\mathbf{u}}{dt} = -\nabla p - \frac{1}{4\pi} \mathbf{B} \times (\nabla \times \mathbf{B}) - \frac{1}{c} \mathbf{j}'_{\text{cr}} \times \mathbf{B} .$$

Defining the MHD energy density $e = \rho u^2/2 + P/(\gamma - 1) + B^2/8\pi$, where γ is the adiabatic index of the background gas, it follows that the energy density also differs from its usual conservative form

$$\frac{\partial e}{\partial t} + \nabla \cdot \left[\left(e + p + \frac{B^2}{8\pi} \right) \mathbf{u} - \frac{1}{4\pi} (\mathbf{u} \cdot \mathbf{B}) \mathbf{B} \right] = -\mathbf{j}'_{\text{cr}} \cdot \mathbf{E} \quad (11)$$

i.e. if the background plasma can set up an electric field to oppose the cosmic ray current, work is done by the cosmic rays on the MHD fluid. Note that there is no need to transform back to the laboratory frame since the return current is always defined locally to oppose that of the cosmic rays.

Since the primary focus of this paper is the growth of magnetic waves and its feedback on the particles driving the growth, we make the following approximations:

(i) To reduce memory requirements and allow for a larger spatial domain as well as larger number of harmonics, we dispense with the momentum grid. This is achieved applying the same technique used in Bell et al. (2011), where a uniform power-law distribution is assumed for all harmonics

$$\frac{\partial f_{\ell}^m}{\partial p} = -s \frac{f_{\ell}^m}{p} \quad (12)$$

This is similar to making a mono-energetic approximation, but ensures the $\mathbf{E} \times \mathbf{B}$ drifts remain properly accounted for. For the parameters we consider, this is the most important effect. To prevent divergence of the cosmic-ray pressure, we have taken the value $s = 4.1$ in all simulations. This also ensures all H_3^m terms (see appendix, equation A5) do not vanish exactly.

(ii) a finite collision frequency $\nu (\ll \Omega)$ is chosen in order to guarantee the closure of the spherical harmonic expansion. As can be seen from the appendix (Eq. A6), in the absence of other effects the high harmonics are damped exponentially

$$f_{\ell}^m(t + \Delta t) = f_{\ell}^m(t) \exp\left(-\frac{\nu}{2} \ell(\ell + 1) \Delta t\right) .$$

It is therefore possible to truncate the harmonic expansion at $\ell = L_{\text{max}}$, subject to the condition that $L_{\text{max}} > \sqrt{\Omega/\nu}$. It will be demonstrated that after the field has been allowed to grow sufficiently, the self-consistent scattering on magnetic field structures dominates the artificial collisions imposed by ν .

(iii) Perhaps the most crucial approximation that we adopt, which is a theoretical tool quite unique to the spherical harmonic expansion technique, is to add an additional term proportional to the large scale gradient of the isotropic part of the spectrum $f_{\text{LS}}(x)$. This results in an additional source term in the $A_{x,1}^0$ expression for f_1^0 (Equation A2), i.e. we include

$$\hat{A}_{x,1}^0 = -c \frac{\partial f_{\text{LS}}}{\partial x} .$$

This term acts like an external driving force, which allows us to model the larger scale dynamics of the precursor. In the absence of self-generated magnetic fields, this term would

allow the system to relax to the standard steady state solution, where advection and diffusion balance. In order to use this approximation, the gradient must vary on scales larger than the length of the simulation domain L_{sim} , ie.

$$f_{\text{LS}} \left/ \left| \frac{\partial f_{\text{LS}}}{\partial x} \right| \right. \gg L_{\text{sim}}$$

Similarly, the use periodic boundary conditions for all other quantities demands that this condition be satisfied, since otherwise the large scale gradient is resolved, and different boundary conditions or full shock simulations are necessary. The gradient that we use in the simulations is taken to be that associated with the steady state solution described in the previous section, where the value of D_{B} is determined from the numerical value for ν used in the simulation.

Previous PIC/Hybrid kinetic simulations of cosmic-ray streaming instabilities including feedback on the driving particles, have suffered from the fact that the energy must be transferred to the background plasma at the expense of the cosmic-ray anisotropy (Lucek & Bell 2000; Stroman et al. 2009; Reville & Bell 2012). Hence, only a finite amount of free energy, determined by the initial conditions, was available in the system to amplify the magnetic field. Bell (2004) circumvented this problem by noting that on scales much less than the gyroradius of the cosmic rays, the feedback on the particles was, at least in the linear theory, negligible, and a constant uniform current could be used. In this paper we bridge the gap between these two regimes, by using the local approximation above, which allows us to control the driving of the cosmic ray current.

4 SIMULATION RESULTS

Despite the fact that a spherical shock expanding into a large scale uniform magnetic field has considerably more of its shock surface at large obliquities, parallel or quasi-parallel shocks have received by far the most attention. This may be largely due to the belief that injection into the acceleration process is suppressed at high Mach number quasi-perpendicular shocks (e.g. Baring et al. 1994). However, observations of supernovae would suggest that this is not the case. Shell-type supernovae are quite abundant in our galaxy, and it is extremely unlikely that these rims represent exclusively quasi-parallel shocks. Kinetic simulations of the shock microphysics are providing new insight (see e.g. Gargate & Spitkovsky 2012; Matsumoto et al. 2012, and references therein), but the solution to the injection problem in its entirety remains unsolved. In the following, we assume that the shock has already put a considerable amount its energy into the cosmic-ray population, but not yet significantly amplified the magnetic fluctuations.

The simulations are performed in three dimensions, using periodic boundary conditions, where the computational domain represents the evolution of a small region at rest in the precursor of a supernova remnant shock. Using the local approximation described in the previous section, we investigate the effect of the angle between the shock normal, as represented by the large scale gradient, and the mean magnetic field. A turbulent component, $\langle \delta B^2 \rangle / B_0^2 \approx 1\%$, is added to the background magnetic field, to seed the growth

of waves. This seeding is essential as VFP codes do not suffer from noise. All simulations begin with the plasma completely at rest, and plasma beta of unity. While the simulations attempt to model as close as possible the parameters relevant for young supernovae, the separation of scales is always a challenge. This manifests itself through the different timescales for the MHD updates, determined by the maximum fast-magnetosonic velocity, and the cosmic-ray velocity, which is essentially the speed of light. Thus the CFL condition on the VFP equation requires a certain amount of sub-cycling. To allow the simulations to run in a reasonable time we are forced to use an initial Alfvén velocity somewhat larger than expected in a real situation, typically $\lesssim 10^{-3}c$. Thus, most of the simulations consider shocks with Alfvén Mach numbers on the order of $M_{\text{A}} \sim 50 - 100$. The code is terminated when the maximum fast magnetosonic speed approaches the speed of light, which usually results due to rapid non-adiabatic heating in the non-linear regime. This non-adiabatic heating may have observational signatures which will be discussed in section 4.3.

4.1 Oblique shocks

The velocity of the intersection point between the shock and a given magnetic field line is $u_{\text{int}} = u_{\text{sh}} / \cos \theta_N$, where θ_N is the angle between the large scale field and the shock normal. If the fields are strongly amplified to values $\delta B / B_0 > 1$, this quantity is, at least locally, quite poorly defined. However, since we start with quite modest fluctuations, we refer to the obliquity with regards initial mean field. Already at $u_{\text{sh}} = c/10$ an angle $\theta_N > 85^\circ$ is required for a superluminal intersection velocity, such that even at quite large obliquities, particles should be able to escape upstream along field-lines.

Starting with the smaller obliquities, figure 1 (a) shows the time evolution of the fluxes and turbulent field component for a shock at an initial angle $\theta_N = 60^\circ$ to the shock normal. The cosmic-ray fluxes grow quickly from zero to match the values predicted from Eq. (8). In fact the peak values correspond almost exactly to these values, suggesting that the diffusion approximation is reasonable at this point, and that the scattering is not yet dominated by the self generated fields. This is to be expected since flux-freezing determines that the fields cannot grow before the plasma is set in motion, so that there is an initial inertial phase where no growth is observed (Bell 2004; Reville et al. 2008), and the cosmic-ray scattering is likewise unaffected in the weak fluctuations. However, once the field starts to grow, the magnitudes of all components of the cosmic-ray current begin to decrease. By the time the field becomes completely disorganised $\delta B \sim B_0$, the shock begins to behave gradually more like a parallel shock, for which the parallel component of the current dominates. This parallel component continues to grow on account of the strong gradient which assumes a fixed value for κ (equation 7) relevant for a 60° angle between the shock normal and the magnetic field.

Increasing the magnetic field angle to 80° , it can be seen that the time evolution of the various components of the current changes slightly, Figure 1 (b). The parallel component is found to grow slowly at first, but then overshoots the value predicted by the diffusion approximation, Eq. (8). The overshoot corresponds approximately to the

fluctuation level where the self-consistent scattering dominates ($\delta B/B_0 > \nu/\Omega$), at which point the cosmic rays diffuse across the field lines more easily. Previous VFP simulations performed by Hornsby et al. (2010), investigating cross field transport in the presence of synthetic turbulence, found that cross field transport approaches the Bohm limit at $\delta B \sim 2B_0$. Returning to the results shown in Figure 1 (b), it is found that the value for j_y also overshoots, while j_z falls short of its predicted value. This is also consistent with a very rapid increase in the collision frequency. This may be due in part to the zero-th order $\mathbf{j}_{cr} \times \mathbf{B}_0$ force accelerating the plasma almost instantly as the angle grows. The currents appear to saturate in a very similar fashion to the previous run at 60° (compare Figures 1 (a) and 1 (b)).

A similar behaviour occurs at the extreme limit of superluminal shock propagation, $\theta_N = 90^\circ$, where both the x and y components of the current overshoot, with j_x gradually increasing into the non-linear regime before saturating, while j_y decreases towards zero, Figure 1 (c). Again, the driving term is fixed in time so the gradient is very steep. The regulation of this gradient is discussed further in section 4.3

In all cases, the final stage of evolution appears to be similar, namely that cosmic rays are prevented from sliding along the field lines, as represented by j_z , while the drifts orthogonal to the plane of the mean field are gradually damped. This suggests a universal behaviour for efficiently accelerating shocks, such that they tend asymptotically towards parallel-like shocks. While this phenomenon has been widely believed to occur, this is the first time that it has been demonstrated in a self-consistent manner. The global effect this has on the acceleration is uncertain at present.

A possible by-product of this behaviour may reveal itself on interaction with the shock surface itself. Previous numerical simulations by Zirakashvili & Ptuskin (2008) demonstrated that for a parallel shock, the non-linear structures generated by the NRH instability can, on crossing the shock, result in stretching of the magnetic component parallel to the shock normal, such that it dominates over the component in the shock plane. We find that similar structures are found in simulations at all obliquities, suggesting that even initially perpendicular shocks may result in radially pointing magnetic fields downstream of young supernova remnant shock, as has been observed in several remnants (Milne 1987).

A caveat regarding the non-linear evolution concerns the finite lifetime of the simulation region, being in the upstream rest-frame, it must at some stage be advected through the shock. This problem is most severe in the case of highly oblique shocks, where the precursor is initially on the order of only a few gyroradii. However, as the magnetic field becomes increasingly disordered, particles will penetrate deeper into the upstream plasma, and allow further time for magnetic field growth. Ultimately, for shocks efficiently accelerating cosmic-rays, self-generated fields take over and the shock will behave more like a parallel shock. However, sufficiently far upstream, the fields will remain regular, at least at the level of pre-existing interstellar turbulence, and particle escape to infinity is impeded. Clearly full shock simulations are required to treat this problem self-consistently. This will be addressed in a follow-up paper.

It is tempting to connect these results to the previous

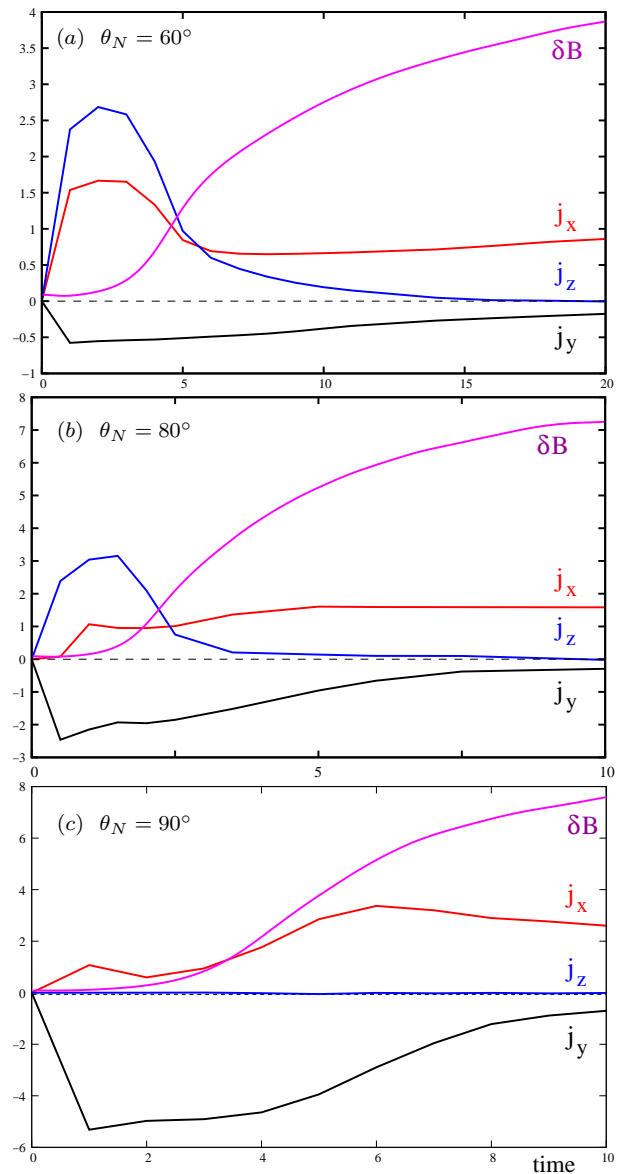


Figure 1. The lab frame current densities $\mathbf{j} = n_{cr}e\mathbf{u} + \mathbf{j}'$ and growth of magnetic field as a function of time. Initial conditions are chosen such that $\nu = 0.1\Omega$, $u_{sh} = 0.03c$. Magnetic field is in units of B_0 . Time units are $20.8/\Omega_0$ i.e. if the CR are at 100 TeV, and $B_0 = 3 \mu\text{G}$, time is approximately in years.

work of Bell et al. (2011), where it was demonstrated that the shape of the non-thermal power law could deviate from the standard test-particle value at oblique shocks, depending on the angle and collision frequency. This deviation is essentially a direct consequence of the inability to match the perpendicular currents across the shock in the diffusion approximation, which demands $f_0(x > 0, p) = \text{const}$. We have just demonstrated that the time-asymptotic state of any efficiently accelerating shock front is one in which the perpendicular currents vanish, which implies the existence of a possible radiative signature that can be used to probe the level of upstream field amplification. To illustrate this point, SN 1987a is taken as an example.

Considering very young supernovae, the results presented here suggest that shocks which are efficiently accel-

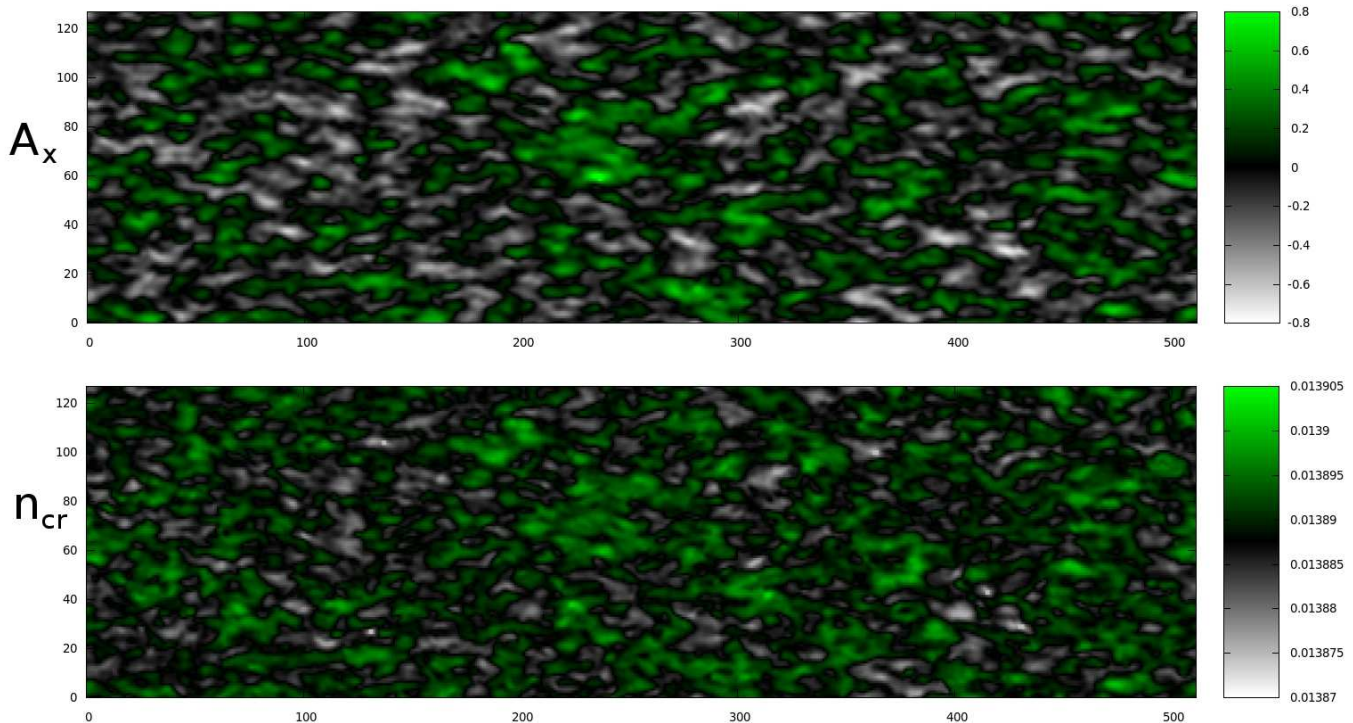


Figure 2. Slice through the $x - y$ plane demonstrating the correlation between A_x and n_{cr} . While this is found to occur at early times, no additional focussing was found in any of the simulations, and the correlation eventually disappears in the non-linear stage.

erating cosmic rays might have an observable time dependent behaviour, as both the cosmic-ray efficiency and self-generated magnetic field fluctuations increase. SN1987a represents an interesting example, since the radio flux has been increasing steadily for over 20 years, implying an increasing acceleration efficiency, while the spectrum has been steadily flattening (Zanardo et al. 2010). Reconciling this behaviour within the non-linear diffusive shock acceleration framework requires a somewhat arbitrary fine-tuning of the electron-proton injection ratio (Berezhko et al. 2011). However, this time-dependent behaviour is quite consistent with acceleration at an oblique shock. Since the shock is believed to be expanding into a Parker spiral (Kirk & Wassmann 1992), at least for some of its lifetime, the majority of the shock surface should have large magnetic obliquities. As the acceleration becomes more efficient, the magnetic fluctuations become amplified, and the collision frequency increases. Comparing to figure 1 of Bell et al. (2011), this will lead to a gradual flattening of the spectrum. As the field enters the non-linear regime of magnetic field amplification, the perpendicular currents are damped near the shock, and a power-law spectrum closer to the standard test-particle result should result. While this explanation is clearly not in any way rigorous, it does provide an alternative to the non-linear shock acceleration model, which neglects the effects of the obliquity of the upstream magnetic fields, and additionally any deviations from the diffusion approximation.

4.2 Parallel shocks

Parallel shocks have received the greatest attention in the literature, both in terms of particle acceleration and resulting magnetic field amplification. We have performed an exten-

sive suite of simulations investigating the growth of magnetic field in this configuration, to investigate a number of effects.

Recently, Reville & Bell (2012) presented a theoretical and numerical investigation of cosmic-ray filamentation and its role in the generation of large scale magnetic fluctuations. The results were based on a two-dimensional analysis that assumed slab-symmetry along the direction of cosmic-ray anisotropy. It was demonstrated that the cosmic-ray density correlates with the component of the magnetic vector potential parallel to the direction of cosmic ray streaming.

Using the VFP code, we are able to drop the approximation of slab symmetry and investigate if the process occurs when the third dimension is included. The code is set up as before, with periodic boundary conditions and a large scale imposed gradient to drive a current consistent with equation (8). It is found in all cases that the cosmic-ray density correlates with the vector potential during the linear growth ($\delta B \ll B_0$) as can be seen in Figure 2. In fact, the correlation also exists at oblique shocks, although the correlation is between the cosmic-ray density and the component of the vector potential parallel to the mean cosmic-ray current. In this sense, the linear analysis of Reville & Bell (2012) still applies, and one might expect growth of large scale fields. However, the resulting filaments that form do not continue to focus, and the structures are ultimately destroyed in the non-linear stage. It should be pointed out that we only consider the evolution of cosmic rays at a single energy, and that the simulation domain is periodic. It is still possible, and in fact quite likely, that the leading edge of the precursor can still filament (see recent results from Caprioli & Spitkovsky (2013)). The periodic simulations presented here are more representative of a region deep in the precursor. An extensive parameter scan failed to produce noticeable elongated

structures in our simulations. On the other hand, the results do seem to suggest that cosmic rays can only escape the source at the highest energies, which is consistent with current models of cosmic-ray escape. Full, energy-dependent shock simulations are still required to rule out the possible significance of cosmic-ray filamentation as a low energy cosmic-ray escape channel.

The simulations allow us also to address, the interaction between the cosmic rays and the self-consistently amplified magnetic fields, over a spatial range that covers both the gyro-resonant interactions and the sub-Larmor scale fluctuations where the fast growing NRH instability operates. A number of interesting effects are found. First, it is noted that the evolution of the plasma is quite different from that typically seen in the fixed cosmic-ray current simulations (Bell 2004; Reville et al. 2008; Zirakashvili et al. 2008). Figure 3 shows the evolution of the different components of the energy. Previous MHD simulations of the field amplification using a constant uniform current typically go through three stages. An initial inertial phase, where the plasma is set in motion, and the magnetic field is either constant or can actually decrease as energy is transferred to the background fluid motions. Once in motion, the plasma starts to stretch the field lines, and reinforced by the $\mathbf{j} \times \mathbf{B}$ force, leads to a run-away instability. Finally, in the non-linear phase, the plasma motion is highly disordered and rotational. The kinetic energy continues to grow as t^2 (Pelletier et al. 2006; Zirakashvili et al. 2008), and the magnetic energy grows in equipartition with the same scaling.

When we include the feedback on cosmic rays, the initial behaviour is the same, but the growth of kinetic energy stagnates at early times. The magnetic field starts to grow, with total energy density in the growing magnetic modes quickly dominating the kinetic energy. Already at $\delta B^2/B_0^2 \sim 0.1$ the scattering on magnetic structures acts to reduce the current such that the driving term can no longer compensate. Eventually, the cosmic-ray current becomes too weak to have any influence on the magnetic field on a timescale comparable with the precursor crossing time.

An interesting result of amplifying the magnetic field on sub-Larmor scales, is that the frequent scattering on the resulting non-linear fluctuations prevents the current from following the field on large scales. This can clearly be seen in Figure 4, where the dominant magnetic field structures are on scales much less than the particle gyroradius which is 3/4 the box length and 3 times the box width. Thus, one can safely assume that the usual expression for the linear growth rate of parallel modes ($\mathbf{k} \parallel \mathbf{B}_0$)

$$\gamma = \sqrt{\frac{k j_{cr} B_0}{\rho c}} \quad (13)$$

holds up to wavelengths larger than the gyroradius of the particles driving the growth. Of course, the simulations are initialised with a perfectly uniform mean field, and variations in the orientation of the large scale magnetic field in the pre-existing ambient circumstellar medium may introduce interesting additional effects (Giacinti et al. 2012). Nevertheless, a faster growth rate at long wavelengths is clearly implied.

The role of collisional effects has also been discussed in Schure & Bell (2011). Whether this is the same insta-

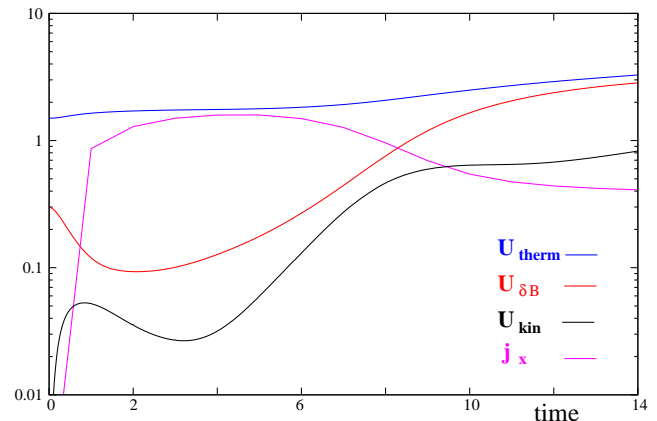


Figure 3. Time evolution of the different components of the energy density. $U_{\delta B} = \langle B^2 - B_0^2 \rangle / 8\pi$ is the energy density in the magnetic fluctuations having subtracted off the energy associated with the mean field. All energy densities are in units $B_0^2 / 8\pi$. (The sharp jump in j_x from $t=0$ to $t=1$ is due to the fact that the current is only stored at integer timesteps.)

bility is uncertain, since non-resonant scattering on short wavelength fluctuations appears to dominate, and unlike the modes analysed in Schure & Bell (2011), the growing waves are exclusively of a single polarisation, rotating in the opposite sense to the cosmic rays in the mean field, i.e. non-resonant.

4.3 Regulated driving

For the simulations reported in the previous sections, a fixed driving term, determined by the initial conditions and our numerical collision term was used (equation 7). Since the purpose of these investigations is to study the interaction of particles with their own self-generated non-linear structures, we naturally expect a reduction in the mean free path, and consequently, for the system we consider, a similar reduction in the current (Figure 3).

At an actual (quasi-parallel) shock, the increased scattering rate would prevent particles escaping far upstream of the shock, and the scaleheight of the precursor would decrease. Thus, it is reasonable to expect that the cosmic-ray gradient and the diffusion might conspire to maintain the total current density at a constant level, i.e.

$$j_{cr} = e \int d^3 p D \frac{\partial f_0}{\partial x} \approx \text{constant} .$$

We have performed simulations where the large scale gradient (the driving term) is increased in such a way as to maintain an approximately constant cosmic-ray current as the field continues to grow. Starting from the usual result, we allow the current to build up to $t = 3$, and store this value as a reference current. As the magnetic fluctuations grow and dominate, the driving term is increased using a normalisation parameter Δ . This parameter then becomes a measure of the effective reduction in the diffusion coefficient $\Delta = D_B / D$, where D_B is the Bohm value determined from the initial conditions, which for the simulations shown has $\nu = \Omega / 8$. It is found that, not only does the diffusion coefficient reduce well below the value imposed by the initial conditions (as expected), but by the end of the simulation,

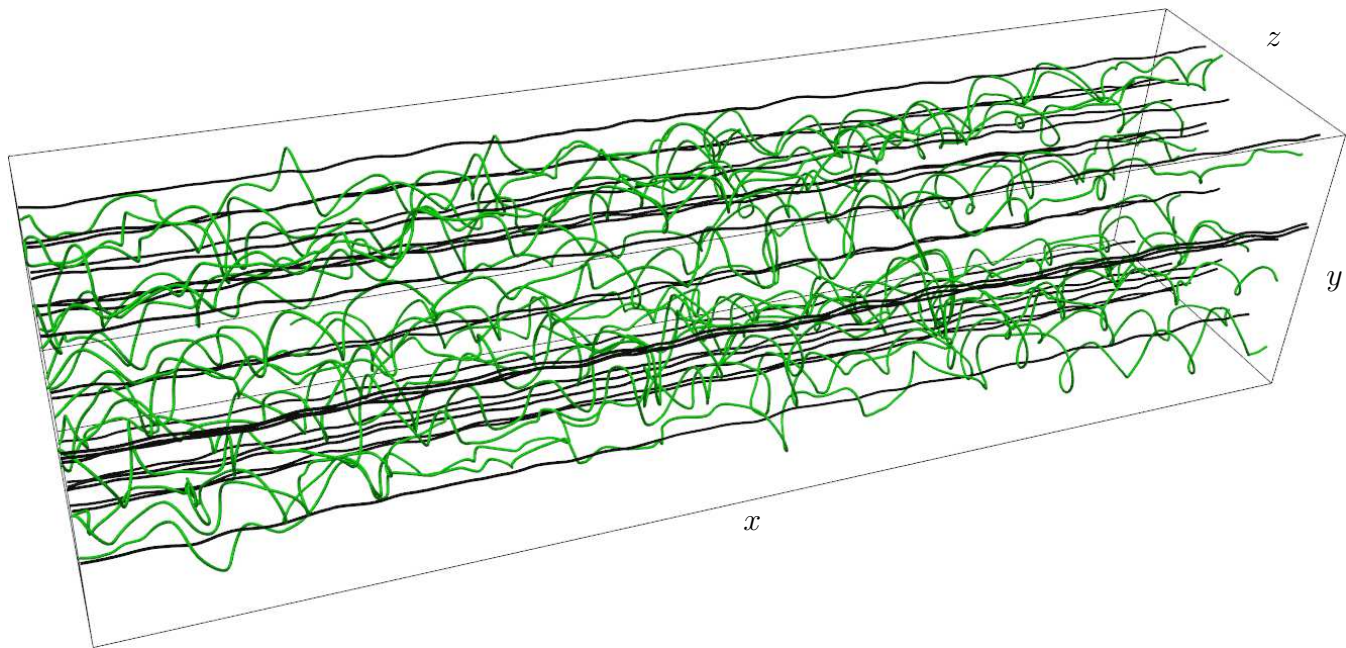


Figure 4. Plot of the field lines for \mathbf{j} and \mathbf{B} from time $t = 10$ for the simulation shown in Figure 3. The approximately straight dark lines correspond to the current, while the green helical lines show the magnetic fieldlines. The gyroradius of the cosmic rays in the mean field is $3/4$ the length of the simulation box.

has even reduced below the Bohm limit in the pre-existing field $\nu_{\text{eff}} \sim 2\Omega$. This can be clearly seen in Figure 6. The simulation is terminated when the maximum fast-magnetosonic velocity becomes comparable with the cell crossing time of the cosmic rays. This happens quite early, due to the artificially large Alfvén velocity used in the simulations. In reality, the fields would continue to grow for considerably longer, as found for example in Bell (2004), and the diffusion coefficient would likely continue to decrease in parallel. We note however, that the scattering is likely dominated by localised regions of very intense magnetic field. At the end of the simulation the magnetic structures are sufficiently strong and on sufficient scale that they can deflect a cosmic ray through $\sim 90^\circ$, as shown in Figure 5.

Since the maximum value of the magnetic field is in general time-limited (saturation of the magnetic field has not been found in any simulation with constant/sustained current), it is expected that the diffusion coefficient of the cosmic-rays will continue to decrease with growing magnetic field, presumably well beyond the level shown here. It is commonly assumed that Bohm diffusion in the amplified magnetic field is an acceptable value for the diffusion coefficient in most calculations of relevance to diffusive shock acceleration. Thus, it is important to be clear about what this means. In section 2, the Bohm scaling argument was derived. Typically when referring to the Bohm limit, it is thought that the collision frequency matches the gyrofrequency, such that

$$D_{\text{B}}^* = \frac{1}{3} \frac{v^2}{\Omega} = \frac{1}{3} r_{\text{g}} v . \quad (14)$$

For highly disordered magnetic fields, confusion can now arise, as it is unclear what value of the magnetic field should be taken when determining the gyroradius, and more importantly, if the Bohm limit itself applies in nature in the

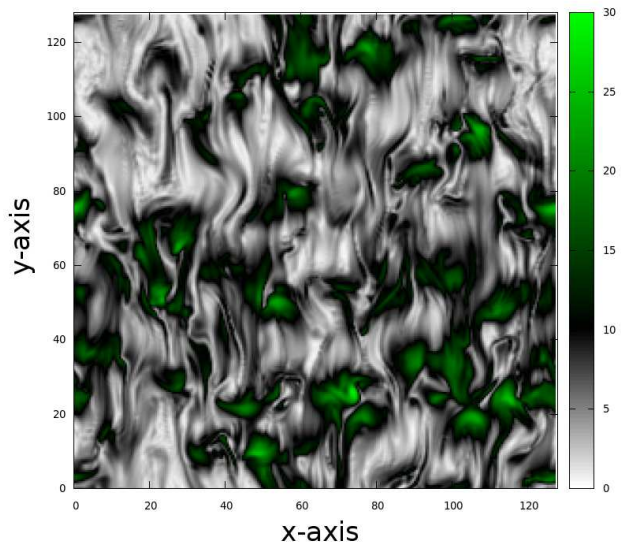


Figure 5. Slice through the x - y plane, showing the magnitude of the magnetic field, in units of B_0 . The regions of intense magnetic field have an average strength of $\sim 25B_0$ and a size $L \sim 10$. The gyroradius of the cosmic rays in the initial field is $r_{\text{g}0} = 256$, such that these regions of intense field can deflect particles through $\Delta\theta \sim L/r_{\text{g}} \sim 90^\circ$.

presence of strong amplification. In the simulations presented here, our experimentally determined diffusion coefficient is half that of the Bohm limit value if we adopt the gyroradius in the pre-amplified magnetic field, but roughly

a factor of four times the Bohm limit in the root mean squared field.² However, the diffusion coefficient was still reducing at the time the simulation was terminated, suggesting that we might expect the diffusion coefficient at a supernova to correspond to its Bohm value in the amplified magnetic field, modulo a numerical factor of order unity. Thus, it may not be such an extreme approximation when considering the maximum energies at young supernovae, to adopt the Bohm limit in the amplified magnetic field, namely the one inferred from observations. Unfortunately, it remains uncertain as to whether the majority of the amplification occurs in the upstream, or acts simply as a seed for Richtmyer-Meshkov type instabilities at the shock front itself (Giagalone & Jokipii 2007; Schure & Bell in prep.). However, as noted by Guo et al. (2012), the growth in the downstream region due to such clumpy interaction occurs over a large distance, and some additional mechanism is required to explain the strong fields observed close to the shock. This favours a scenario in which at least a sizeable fraction of the amplification occurs upstream. Future simulations that include a shock in the simulations will shed further light on this issue.

Finally we note that young supernovae having clear Balmer emission from the outer shock may be used as an indirect probe of upstream amplification. All of the simulations, independent of magnetic obliquity show a common feature, namely that in the non-linear regime, the thermal energy density is greater than the magnetic energy density by typically an order of magnitude, e.g. Figure 6. Thus, if fields of $100\mu\text{G}$ are produced upstream, a thermal energy density in excess of 1 keV/cc may also be produced. The survival of neutrals in such high temperature plasmas is highly unlikely, unless the precursor is very short. However, a short precursor will not provide sufficient time to amplify fields to such high values. Several young remnants show regions of both non-thermal x-ray filaments, synonymous with efficient particle acceleration, and broad/narrow H α emission, suggesting survival of neutrals into the downstream (e.g. Winkler & Long 1997; Ghavamian et al. 2001; Helder et al. 2009). If indeed the magnetic fields are produced predominantly upstream, these regions should anti-correlate, thus providing indirect evidence of in-situ acceleration of cosmic ray protons or nuclei, or indeed the lack thereof. Further observations are necessary to answer this question.

5 DISCUSSION

We have presented a series of numerical simulations investigating the interaction between cosmic rays and magnetic fields in the precursors of supernova remnants. The investigations are carried out using a hybrid MHD-kinetic code which applies a spherical harmonic expansion of the Vlasov-Fokker-Planck equation. This code allows us to consider a range of multi-scale phenomena previously inaccessible to

² This applies only to the particles driving the field growth within our mono-energetic approximation. Previous work by Reville et al. (2008) have already demonstrated the energy dependence of the transport properties in self generated turbulence when the particles were all at considerably lower energies than those assumed driving the field growth.

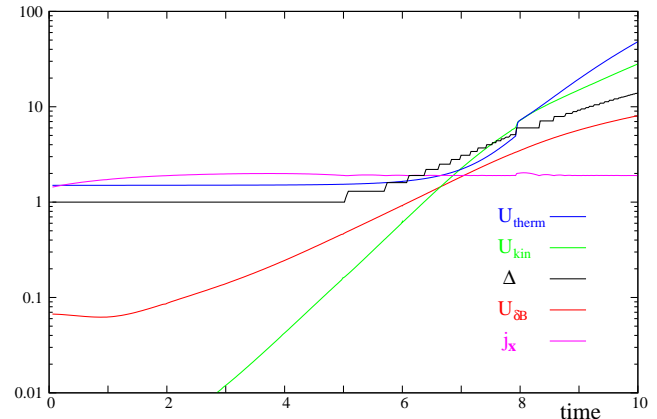


Figure 6. Growth of the different components of the energy density as a function of time for simulations with regulated driving. The current density j_x and Δ the renormalisation parameter of the driving are also shown. $\nu = 0.125\Omega_0$, $u_{\text{sh}} = 0.1c$. Time units are $5.2/\Omega_0$

numerical simulations. A number of results have followed from these simulations that can be applied to existing theories of particle acceleration, and in particular the observational signatures of efficient acceleration at young supernova remnants.

Previous work by Reville & Bell (2012) proposed a method whereby low energy cosmic rays could escape the remnant via self-focussing into low density cavities surrounded by strong magnetic fields. The analysis and simulations performed in Reville & Bell (2012) were exclusively in a 2D slab geometry, which limited the amount of focusing that could be achieved. This is a consequence of the conservation of the component of the vector potential into the plane in such a geometry. Including the third dimension allows for growth of this component, and in theory, continued focusing, which could result in formation of filamentary structures aligned along the direction of cosmic-ray streaming. The current 3D simulations appear to support the linear analysis of Reville & Bell (2012), but that the resulting structures become disrupted over a short distance. While this disfavors the possibility of non-diffusive escape channels for cosmic rays from the remnants, it does provide convincing evidence that the escape of cosmic rays into the interstellar medium at quasi-parallel shocks is limited to a narrow window around the maximum energy, consistent with current models.

Oblique and perpendicular shocks present a slightly different view, although there is clear evidence for a universal behaviour closer to the shock. Far upstream of the shock, where the scattering is weak, particles are tied to field-lines, and advected back towards the shock. It is demonstrated however, that the self-generated fields closer to the shock act to damp any diamagnetic-currents and in a sense, behave very much like parallel shocks. At the same time, considerable amplification of the magnetic field can occur. Previous suggestions that quasi-perpendicular shocks are faster accelerators have implicitly assumed that the scattering was weak (Jokipii 1987). Later calculations demonstrated that the maximum energy became a problem of geometry rather than time (Achterberg 2004; Bell 2008), as the energisation relies on drifting along the shock surface. On the global scale

of the precursor, we now have a rather unusual situation, quite distinct from parallel shocks, where the particles can diffuse isotropically close to the shock, but are strongly confined by the upstream undisturbed field. Whether this acts to increase or decrease the maximum energy is not immediately clear. However, full shock simulations will be performed to answer this question in the near future.

Oblique shocks may also play an important role in explaining observations from young supernovae, or likewise, early observations can provide important information on the acceleration process. Immediately after break-out, supernovae typically expand into a progenitor wind. It is usually assumed in such winds that the radial magnetic field falls off quite rapidly, while the perpendicular component will persist. Thus young supernovae provide ideal laboratories to investigate many of the ideas presented here. We have demonstrated, albeit in a very qualitative sense, how the current evolution of SN 1987a can be explained within the framework of acceleration at highly oblique shocks without the need for non-linear cosmic-ray pressure feedback.

The possibility of sub-Bohm diffusion (with respect to the pre-existing ambient field strength) of cosmic rays at the highest energies has been demonstrated self-consistently for parallel shocks, under the assumption that the driving regulates itself. On the other hand, the normal component of the diffusion tensor at oblique shocks is initially sub-Bohm, but tends to increase due to amplification of magnetic perturbations. Regulation is more complicated in these geometries, and full shock simulations are required. However, the high resolution simulations presented in this paper, show that the self-generated fields naturally produce highly disordered field lines strongly suggesting a universal behaviour of isotropic diffusion at shocks that are efficiently accelerating cosmic rays.

ACKNOWLEDGEMENTS

The research leading to these results has received funding from the European Research Council under the European Community's Seventh Framework Programme (FP7/2007-2013) / ERC grant agreement no. 247039. BR thanks M. Tzoufras and C. Ridgers for valuable discussions on VFP codes, and G. Giacinti for helpful comments on the paper.

REFERENCES

- Achterberg A., 1983, *A&A*, 119, 274
 Achterberg A., 2004, in Beskin V., Henri G., Menard F., et al. eds, *Accretion Discs, Jets and High Energy Phenomena in Astrophysics Course 7: Cosmic Rays and Particle Acceleration at Astrophysical Shocks*. pp 313–401
 Achterberg A., Blandford R. D., Reynolds S. P., 1994, *A&A*, 281, 220
 Bamba A., Yamazaki R., Yoshida T., Terasawa T., Koyama K., 2005, *ApJ*, 621, 793
 Baring M. G., Ellison D. C., Jones F. C., 1994, *ApJS*, 90, 547
 Bell A. R., 2004, *MNRAS*, 353, 550
 Bell A. R., 2005, *MNRAS*, 358, 181
 Bell A. R., 2008, *MNRAS*, 385, 1884
 Bell A. R., Robinson A. P. L., Sherlock M., Kingham R. J., Rozmus W., 2006, *Plasma Physics and Controlled Fusion*, 48, 37
 Bell A. R., Schure K. M., Reville B., 2011, *MNRAS*, 418, 1208
 Berezhko E. G., Ksenofontov L. T., Völk H. J., 2011, *ApJ*, 732, 58
 Caprioli D., Spitkovsky A., 2013, arXiv:1211.6765
 Chandrasekhar S., 1943, *Reviews of Modern Physics*, 15, 1
 Gargaté L., Spitkovsky A., 2012, *ApJ*, 744, 67
 Ghavamian P., Raymond J., Smith R. C., Hartigan P., 2001, *ApJ*, 547, 995
 Giacalone J., Jokipii J. R., 2007, *ApJ*, 663, L41
 Giacinti G., Kachelrieß M., Semikoz D. V., 2012, *Physical Review Letters*, 108, 261101
 Guo F., Li S., Li H., Giacalone J., Jokipii J. R., Li D., 2012, *ApJ*, 747, 98
 Helder E. A., Vink J., Bassa C. G., Bamba A., Bleeker J. A. M., Funk S., Ghavamian P., van der Heyden K. J., Verbunt F., Yamazaki R., 2009, *Science*, 325, 719
 Hornsby W. A., Bell A. R., Kingham R. J., Dendy R. O., 2010, *Plasma Physics and Controlled Fusion*, 52, 075011
 Johnston T. W., 1960, *Phys. Rev.*, 120, 1103
 Jokipii J. R., 1987, *ApJ*, 313, 842
 Kirk J. G., 1994, in Kirk J. G., Melrose D. B., Priest E. R., Benz A. O., Courvoisier T. J.-L., eds, *Saas-Fee Advanced Course 24: Plasma Astrophysics Particle Acceleration (With 26 figures)*. p. 225
 Kirk J. G., Wassmann M., 1992, *A&A*, 254, 167
 Lucek S. G., Bell A. R., 2000, *MNRAS*, 314, 65
 Matsumoto Y., Amano T., Hoshino M., 2012, *ApJ*, 755, 109
 Milne D. K., 1987, *Australian Journal of Physics*, 40, 771
 Pelletier G., Lemoine M., Marcowith A., 2006, *A&A*, 453, 181
 Rakowski C. E., Laming J. M., Hwang U., Eriksen K. A., Ghavamian P., Hughes J. P., 2011, *ApJ*, 735, L21+
 Reville B., Bell A. R., 2012, *MNRAS*, 419, 2433
 Reville B., O'Sullivan S., Duffy P., Kirk J. G., 2008, *MNRAS*, 386, 509
 Schure K. M., Bell A. R., 2011, *MNRAS*, 418, 782
 Schure K. M., Bell A. R., in prep.,
 Skilling J., 1975, *MNRAS*, 172, 557
 Stroman T., Pohl M., Niemiec J., 2009, *ApJ*, 706, 38
 Tzoufras M., Bell A. R., Norreys P. A., Tsung F. S., 2011, *Journal of Computational Physics*, 230, 6475
 Vink J., Laming J. M., 2003, *ApJ*, 584, 758
 Winkler P. F., Long K. S., 1997, *ApJ*, 491, 829
 Zachary A. L., 1987, PhD thesis, California Univ., Berkeley.
 Zanzardo G., Staveley-Smith L., Ball L., Gaensler B. M., Kesteven M. J., Manchester R. N., Ng C.-Y., Tzioumis A. K., Potter T. M., 2010, *ApJ*, 710, 1515
 Zirakashvili V. N., Ptuskin V. S., 2008, *ApJ*, 678, 939
 Zirakashvili V. N., Ptuskin V. S., Völk H. J., 2008, *ApJ*, 678, 255

APPENDIX A: SPHERICAL HARMONIC EXPANSION OF VLASOV-FOKKER-PLANCK EQUATION

In the following, we choose the polar axis to lie along the x -direction, such that the Cartesian momentum vector expressed in terms of spherical angles is $\mathbf{p} = (p \cos \theta, p \sin \theta \cos \phi, p \sin \theta \sin \phi)$. Using the recursion relations and orthogonality condition of the spherical harmonics, the time derivative for each component of the expansion can be written in the form

$$\frac{\partial f_\ell^m}{\partial t} - U_{x,\ell}^m - U_{y,\ell}^m - U_{z,\ell}^m - A_{x,\ell}^m - A_{y,\ell}^m - A_{z,\ell}^m - B_{x,\ell}^m - B_{y,\ell}^m - B_{z,\ell}^m - E_{x,\ell}^m - E_{y,\ell}^m - E_{z,\ell}^m - \sum_{x,y,z} T_{\alpha\beta,\ell}^m = C_\ell^m \quad (\text{A1})$$

Most of these terms have been previously given in Bell et al. (2006) and Tzoufras et al. (2011), but are repeated here so all the equations can be found in one place. The mixed coordinate frame introduces several additional terms, contained in the $T_{\alpha\beta,\ell}^m$, which can be associated with the adiabatic term in equation (1) in the main text. The subscripts $\alpha, \beta \in \{x, y, z\}$ correspond to the relevant term containing the partial derivative $\partial u_\alpha / \partial x_\beta$. Although cumbersome, the derivation of each term is straightforward, and the final expression often displays a noticeable symmetry, a clear indication of the applicability of spherical harmonics in solving problems of this nature.

The advection terms are as follows

$$\begin{aligned} U_{i,\ell}^m &= -u_i \frac{\partial f_\ell^m}{\partial x_i} \quad \forall i \in \{x, y, z\} \\ A_{x,\ell}^m &= -v \frac{\partial}{\partial x} \left[\frac{\ell - m}{2\ell - 1} f_{\ell-1}^m + \frac{\ell + m + 1}{2\ell + 3} f_{\ell+1}^m \right] \\ A_{y,\ell}^{m>0} + A_{z,\ell}^{m>0} &= -\frac{v}{2} D^+ \left[\frac{(\ell - m)(\ell - m - 1)}{2\ell - 1} f_{\ell-1}^{m+1} - \frac{(\ell + m + 1)(\ell + m + 2)}{2\ell + 3} f_{\ell+1}^{m+1} \right] \\ &\quad + \frac{v}{2} D^- \left[\frac{1}{2\ell - 1} f_{\ell-1}^{m-1} - \frac{1}{2\ell + 3} f_{\ell+1}^{m-1} \right] \\ A_{y,\ell}^0 + A_{z,\ell}^0 &= -\Re \left\{ v D^+ \left[\frac{\ell(\ell - 1)}{2\ell - 1} f_{\ell-1}^1 - \frac{(\ell + 1)(\ell + 2)}{2\ell + 3} f_{\ell+1}^1 \right] \right\} \end{aligned} \quad (\text{A2})$$

where $D^\pm = \frac{\partial}{\partial y} \pm i \frac{\partial}{\partial z}$.

Defining the cyclotron rotation vector $\boldsymbol{\Omega} = q\mathbf{B}/\gamma mc$, with q the particle's charge and γm its (relativistic) mass, the rotational terms associated with the magnetic field components are

$$\begin{aligned} B_\ell^{m>0} &= i\Omega_x m f_\ell^m + \frac{1}{2} [(\Omega_z + i\Omega_y) f_\ell^{m-1} - (\ell + m + 1)(\ell - m)(\Omega_z - i\Omega_y) f_\ell^{m+1}] \\ B_\ell^0 &= -\ell(\ell + 1) \Re [(\Omega_z - i\Omega_y) f_\ell^1] \end{aligned} \quad (\text{A3})$$

The spherical harmonic expansion has the additional feature that the rotational terms are algebraic, and do not involve partial derivatives, as would be the case for a Cartesian tensor expansion (Johnston 1960).

Recalling that in the mixed coordinate frame, the local acceleration has an equivalent form to the electric field in the standard Vlasov equation, we thus use the notation

$$\mathbf{E} = \frac{1}{c} \left[\frac{\partial \mathbf{u}}{\partial t} + (\mathbf{u} \cdot \nabla) \mathbf{u} \right],$$

from which it follows

$$\begin{aligned} E_{x,\ell}^m &= E_x p \left[\frac{\ell - m}{2\ell - 1} G_{\ell-1}^m + \frac{\ell + m + 1}{2\ell + 3} H_{\ell+1}^m \right] \\ E_{y,\ell}^{m>0} + E_{z,\ell}^{m>0} &= -\frac{p}{2} \left[\frac{E_y - iE_z}{2\ell - 1} G_{\ell-1}^{m-1} - \frac{E_y + iE_z}{2\ell - 1} (\ell - m)(\ell - m - 1) G_{\ell-1}^{m+1} \right. \\ &\quad \left. - \frac{E_y - iE_z}{2\ell + 3} H_{\ell+1}^{m-1} + \frac{E_y + iE_z}{2\ell + 3} (\ell + m + 1)(\ell + m + 2) H_{\ell+1}^{m+1} \right] \\ E_{y,\ell}^0 + E_{z,\ell}^0 &= \Re \left\{ p(E_y + iE_z) \left[\frac{\ell(\ell - 1)}{2\ell - 1} G_{\ell-1}^1 - \frac{(\ell + 1)(\ell + 2)}{2\ell + 3} H_{\ell+1}^1 \right] \right\} \end{aligned} \quad (\text{A4})$$

where

$$G_\ell^m = p^\ell \frac{\partial}{\partial p} \left(p^{-\ell} f_\ell^m \right), \quad H_\ell^m = p^{-(\ell+1)} \frac{\partial}{\partial p} \left(p^{(\ell+1)} f_\ell^m \right) \quad (\text{A5})$$

Since the adiabatic term has two occurrences of the momentum vector, it contains nine different terms associated with the different combinations of the axes. However, due to the symmetry about the polar axis, most of these terms are very similar and can be grouped together. Some of these terms have been previously derived in one (Bell et al. 2011) and two dimensions

(C. Ridgers private communication).

$$\begin{aligned}
T_{xx,\ell}^m &= p \frac{\partial u_x}{\partial x} \left[\frac{(\ell-m)(\ell-m-1)}{(2\ell-3)(2\ell-1)} G_{\ell-2}^m + \frac{(\ell-m+1)(\ell+m+1)}{(2\ell+3)(2\ell+1)} G_\ell^m \right. \\
&\quad \left. + \frac{(\ell+m)(\ell-m)}{(2\ell+1)(2\ell-1)} H_\ell^m + \frac{(\ell+m+1)(\ell+m+2)}{(2\ell+3)(2\ell+5)} H_{\ell+2}^m \right] \\
T_{xy,\ell}^{m>0} + T_{xz,\ell}^{m>0} &= \frac{p}{2} \left(\frac{\partial u_x}{\partial y} - i \frac{\partial u_x}{\partial z} \right) \left[\frac{\ell+m+1}{(2\ell+5)(2\ell+3)} H_{\ell+2}^{m-1} \right. \\
&\quad \left. + \frac{\ell-m+2}{(2\ell+1)(2\ell+3)} G_\ell^{m-1} - \frac{\ell+m-1}{(2\ell+1)(2\ell-1)} H_\ell^{m-1} - \frac{\ell-m}{(2\ell-1)(2\ell-3)} G_{\ell-2}^{m-1} \right] \\
&\quad + \frac{p}{2} \left(\frac{\partial u_x}{\partial y} + i \frac{\partial u_x}{\partial z} \right) \left[- \frac{(\ell+m+1)(\ell+m+2)(\ell+m+3)}{(2\ell+5)(2\ell+3)} H_{\ell+2}^{m+1} \right. \\
&\quad \left. - \frac{(\ell-m)(\ell+m+1)(\ell+m+2)}{(2\ell+1)(2\ell+3)} G_\ell^{m+1} + \frac{(\ell-m)(\ell+m+1)(\ell-m-1)}{(2\ell+1)(2\ell-1)} H_\ell^{m+1} \right. \\
&\quad \left. + \frac{(\ell-m)(\ell-m-1)(\ell-m-2)}{(2\ell-1)(2\ell-3)} G_{\ell-2}^{m+1} \right] \\
T_{xy,\ell}^0 + T_{xz,\ell}^0 &= p \Re \left\{ \left(\frac{\partial u_x}{\partial y} + i \frac{\partial u_x}{\partial z} \right) \left[- \frac{(\ell+1)(\ell+2)(\ell+3)}{(2\ell+5)(2\ell+3)} H_{\ell+2}^1 \right. \right. \\
&\quad \left. \left. - \frac{\ell(\ell+1)(\ell+2)}{(2\ell+1)(2\ell+3)} G_\ell^1 + \frac{\ell(\ell+1)(\ell-1)}{(2\ell+1)(2\ell-1)} H_\ell^1 + \frac{\ell(\ell-1)(\ell-2)}{(2\ell-1)(2\ell-3)} G_{\ell-2}^1 \right] \right\}
\end{aligned}$$

$$\begin{aligned}
T_{yx,\ell}^{m>0} + T_{zx,\ell}^{m>0} &= \frac{p}{2} \partial_x (u_y - i u_z) \left[\frac{\ell+m+1}{(2\ell+5)(2\ell+3)} H_{\ell+2}^{m-1} \right. \\
&\quad \left. - \frac{\ell+m+1}{(2\ell+1)(2\ell+3)} G_\ell^{m-1} + \frac{\ell-m}{(2\ell+1)(2\ell-1)} H_\ell^{m-1} - \frac{\ell-m}{(2\ell-1)(2\ell-3)} G_{\ell-2}^{m-1} \right] \\
&\quad + \frac{p}{2} \partial_x (u_y + i u_z) \left[- \frac{(\ell+m+1)(\ell+m+2)(\ell+m+3)}{(2\ell+5)(2\ell+3)} H_{\ell+2}^{m+1} \right. \\
&\quad \left. + \frac{(\ell-m)(\ell+m+1)(\ell-m+1)}{(2\ell+1)(2\ell+3)} G_\ell^{m+1} - \frac{(\ell-m)(\ell+m+1)(\ell+m)}{(2\ell+1)(2\ell-1)} H_\ell^{m+1} \right. \\
&\quad \left. + \frac{(\ell-m)(\ell-m-1)(\ell-m-2)}{(2\ell-1)(2\ell-3)} G_{\ell-2}^{m+1} \right] \\
T_{yx,\ell}^0 + T_{zx,\ell}^0 &= p \Re \left\{ \partial_x (u_y + i u_z) \left[- \frac{(\ell+1)(\ell+2)(\ell+3)}{(2\ell+5)(2\ell+3)} H_{\ell+2}^1 \right. \right. \\
&\quad \left. \left. + \frac{\ell(\ell+1)^2}{(2\ell+1)(2\ell+3)} G_\ell^1 - \frac{\ell^2(\ell+1)}{(2\ell+1)(2\ell-1)} H_\ell^1 + \frac{\ell(\ell-1)(\ell-2)}{(2\ell-1)(2\ell-3)} G_{\ell-2}^1 \right] \right\}
\end{aligned}$$

$$T_{yy,\ell}^m + T_{yz,\ell}^m + T_{zy,\ell}^m + T_{zz,\ell}^m = Q_\ell^m + R_\ell^m + S_\ell^m$$

where

$$\begin{aligned}
Q_\ell^{m>1} &= pY \left[\frac{1}{(2\ell+3)(2\ell+5)} H_{\ell+2}^{m-2} - \frac{1}{(2\ell-1)(2\ell+1)} H_\ell^{m-2} - \frac{1}{(2\ell+1)(2\ell+3)} G_\ell^{m-2} + \frac{1}{(2\ell-3)(2\ell-1)} G_{\ell-2}^{m-2} \right] \\
S_\ell^m &= pY^* \left[\frac{(\ell+m+1)(\ell+m+2)(\ell+m+3)(\ell+m+4)}{(2\ell+3)(2\ell+5)} H_{\ell+2}^{m+2} - \frac{(\ell-m)(\ell-m-1)(\ell+m+1)(\ell+m+2)}{(2\ell-1)(2\ell+1)} H_\ell^{m+2} \right. \\
&\quad \left. - \frac{(\ell-m)(\ell-m-1)(\ell+m+1)(\ell+m+2)}{(2\ell+1)(2\ell+3)} G_\ell^{m+2} + \frac{(\ell-m)(\ell-m-1)(\ell-m-2)(\ell-m-3)}{(2\ell-3)(2\ell-1)} G_{\ell-2}^{m+2} \right] \\
R_\ell^m &= \frac{p}{2} \left(\frac{\partial u_y}{\partial y} + \frac{\partial u_z}{\partial z} \right) \left[\frac{(\ell+1)(\ell+2)+m^2}{(2\ell+1)(2\ell+3)} G_\ell^m + \frac{\ell(\ell-1)+m^2}{(2\ell+1)(2\ell-1)} H_\ell^m \right. \\
&\quad \left. - \frac{(\ell-m)(\ell-m-1)}{(2\ell-1)(2\ell-3)} G_{\ell-2}^m - \frac{(\ell+m+1)(\ell+m+2)}{(2\ell+5)(2\ell+3)} H_{\ell+2}^m \right] + i \frac{p}{2} \left(\frac{\partial u_y}{\partial z} - \frac{\partial u_z}{\partial y} \right) \frac{m}{2\ell+1} [G_\ell^m - H_\ell^m]
\end{aligned}$$

where

$$Y = \frac{1}{4} \left(\frac{\partial u_y}{\partial y} - \frac{\partial u_z}{\partial z} \right) - i \frac{1}{4} \left(\frac{\partial u_y}{\partial z} + \frac{\partial u_z}{\partial y} \right)$$

For $m < 2$ we have $Q_\ell^0 = (S_\ell^0)^*$ and

$$Q_\ell^1 = pY \left[\frac{\ell(\ell+1)}{(2\ell-1)(2\ell+1)} (H_\ell^1)^* - \frac{(\ell+2)(\ell+3)}{(2\ell+3)(2\ell+5)} (H_{\ell+2}^1)^* + \frac{\ell(\ell+1)}{(2\ell+1)(2\ell+3)} (G_\ell^1)^* - \frac{(\ell-2)(\ell-1)}{(2\ell-3)(2\ell-1)} (G_{\ell-2}^1)^* \right]$$

Finally, since the spherical harmonics are themselves solutions to Laplace's equation, the collision term takes a particularly simple form

$$C_\ell^m = -\frac{\nu}{2} \ell(\ell+1) f_\ell^m \tag{A6}$$

This paper has been typeset from a $\text{\TeX}/\text{\LaTeX}$ file prepared by the author.